PRELIMINARY ANALYSIS OF LDEF INSTRUMENT A0187-1 "CHEMISTRY OF MICROMETEOROIDS EXPERIMENT"

Friedrich Hörz
NASA Johnson Space Center
Solar System Exploration Division
Houston, Texas 77058

Ronald P. Bernhard, Jack Warren, Thomas H. See
Lockheed Engineering & Sciences Company
Houston, Texas 77058

Donald E. Brownlee, Mark R. Laurance, Scott Messenger
Department of Astronomy
University of Washington
Seattle, Washington 98195

Robert B. Peterson
3738 Arnold Street
Houston, Texas 77005

SUMMARY

The "Chemistry of Micrometeoroids Experiment" (CME) exposed approximately 0.8 m^2 of gold (>99.99% pure) on LDEF's trailing edge (location A03) and approximately 1.1 m^2 aluminum (>99%) in the forward-facing A11 location. Detailed crater counts reveal a factor of 7-8 enhancement of the effective particle flux on the A11 location compared to LDEF's trailing edge. These differences are in qualitative agreement with recent theoretical models regarding dynamic properties of hypervelocity particles in low-Earth orbit.

Survey-type, compositional investigations of the impactor population(s) via electron beam methods and associated energy dispersive X-ray analysis have commenced. A large fraction (>50%) of all craters retain projectile masses below the sensitivity threshold of the SEM methods used. Projectile residues that can be analyzed may be classified into "natural" and "man-made" sources, yet our investigations have not progressed to the point where we can define their relative abundance with confidence. Most large craters seem to have been caused by natural impactors, however.

The most significant results to date relate to the discovery of unmelted pyroxene and olivine fragments associated with natural cosmic dust impacts; the latter are sufficiently large (μm) for detailed phase studies and they serve to demonstrate that recovery of unmelted dust fragments is a realistic prospect for future dust experiments that will employ more advanced collector media. We also discovered that man-made debris impacts occur on LDEF's trailing edge with substantially higher frequency than expected, suggesting that orbital debris in highly elliptical orbits may have been somewhat underestimated. Even these preliminary results illustrate the great potential of LDEF to contribute to ongoing studies of extraterrestrial materials, as well as to an improved understanding of collisional hazards in LEO.

INTRODUCTION

LDEF experiment A0187-1, the "Chemistry of Micrometeoroid Experiment" (CME) occupied two full LDEF trays, located on Rows 3 and 11. Its primary purpose was to retrieve analyzable projectile residue associated with hypervelocity craters in infinite halfspace targets. The most prolific sources of natural dust are asteroids and comets, which are primitive solar system objects that escaped the pervasive thermal processing of the inner planets. Therefore, the chemical information extracted from natural impactors will yield insight into early solar system processes. Even more so if unmelted particle fragments were found to characterize textural relationships and individual minerals. The unexpectedly long duration of the LDEF mission, some 5.7 years, enhanced these opportunities beyond expectation.

In addition, substantial developments since the inception of the LDEF experiments provide new opportunities, and a much improved interpretative context for the initial objectives. Three significant developments occurred. First, the

existence and significance of interplanetary dust was recognized in particle collections obtained from the stratosphere by high altitude aircraft (ref. 1), in deep-sea sediments and in pre-industrial polar ices (ref. 2). Also, greatly improved or innovative analytical methods enabled detailed mineralogical, chemical and isotopic investigations, rendering laboratory analysis of interplanetary dust into an integral and highly rewarding part of extraterrestrial materials research (*e.g.*, refs. 2, 3, 4, 5). Second, a number of dust instruments were onboard the GIOTTO and VEGA spacecraft as they passed close to comet Halley in 1986. Highly successful mass spectrometers provided the first *in situ* chemical analyses of cometary solids (*e.g.*, ref. 6). Many Halley particles seem to be akin to those collected in the stratosphere, but not all. Third, awareness of a substantial collisional threat in Earth orbit from man-made debris increased over the past decade, and vigorous efforts have been initiated, at international levels, to better understand and cope with this hazard (ref. 7).

Based on these developments during the past decade, an understanding of LDEF's impact record has assumed increased significance. Are terrestrial collections of interplanetary dust representative or does heating during atmospheric entry introduce bias? What are the impact rates of natural particles versus man-made debris? What are the most prolific sources of man-made particles? The detailed analysis of our CME experiment intends to contribute to these questions. The following is a progress report toward that objective.

INSTRUMENT DESCRIPTION

The CME exposed two substantially different instruments, one containing movable collector surfaces (*i.e.*, the "active" instrument), the other was totally "passive". Their salient features and underlying rationale are described below. The active tray was considered the potentially more valuable collector and was therefore located on LDEF's trailing edge which was expected to be the least contaminated LDEF location. Also, relative encounter speeds are the lowest in the rearwards-facing direction compared to any other LDEF location, as detailed below.

Figure 1. The CME experiment trays during retrieval operations by STS 32. (A) The active experiment on LDEF location A03 (trailing edge), exposing seven plates of gold (approximately 0.8 m^2) and some auxiliary surfaces to evaluate their suitability as micrometeoroid collectors. Note the "open" configuration of the clamshell devices. (B) "Passive" tray, located in the forward-facing A11 location and exposing 6 plates of >99% pure aluminum (1100 series), approximately 1.1 m^2 in total surface area.

Active Instrument (Tray A03)

The active instrument occupied an entire 12" deep tray located in Bay A03 and exposed seven sheets (~0.5 mm thick) of pure gold (>99.99% Au), each sheet measuring approximately 57 x 20 cm (Figure 1a). Accounting for fasteners and clamping devices, each sheet exposed approximately 1170 cm^2 for a cumulative surface area of 0.82 m^2. The rationale for selecting gold as collector substrate was as follows: Au has a characteristic X-ray spectrum that does not seriously interfere with most elements of interest during energy-dispersive analyses using electron beam methods for excitation. Also, a prerequisite for any collector medium is that it not contain elements of cosmochemical significance and Au is not a terribly diagnostic element to distinguish among diverse classes of extraterrestrial materials. The high malleability of gold leads to relatively large craters, again a favorable property. The major drawback of gold is its high density, leading to substantial shock stresses and unfavorably high temperatures during hypervelocity impacts compared to target materials of lower bulk density.

A fraction of the active CME tray, totalling approximately 1100 cm^2, was occupied by eight experimental surfaces, each about 20 x 7 cm in size but of variable thickness to empirically determine their suitability for hypervelocity particle capture (Figure 1a). They included other high-purity, mono-elemental collector plates (Al, Be, Ti, Zn, C), Kapton, and low-density, porous Teflon filters, the latter intended to impart the least shock stresses for possible recovery of unmelted particle remnants (refs. 8,9). None of these experimental surfaces have been analyzed in detail.

Figure 1a depicts the active instrument during retrieval operations in low-Earth orbit (LEO). The most noteworthy feature in Figure 1, other than the detailed geometry and arrangements, relates to the "opened" and exposed gold collectors. The gold actually occupied the insides of clamshell-type devices that opened and closed upon self-contained command. The rationale for such "active" clamshells was to protect the ultra-clean gold surfaces from contamination during all nominal ground handling and on-orbit Shuttle operations. A mechanical labyrinth seal protected the collectors from particulate contaminants in closed position, yet not from gaseous species. Under nominal operations, the clamshells should have opened about 10 days after LDEF deployment, and closed a similar period prior to the scheduled retrieval by the Shuttle 9 months later. These operations had to be preprogrammed relative to the nominal LDEF mission. In Appendix A, we detail our findings regarding the open clamshell configuration, possibly caused by a malfunctioning closing mechanism during the unexpectedly long exposure in LEO. We conclude that the instrument worked nominally throughout the entire LDEF mission and that the clamshells opened and closed repeatedly, and as designed, until actual retrieval after 5.7 years.

Passive Instrument (Tray A11)

Total instrument resources were insufficient to have two (or more) LDEF trays equipped with active clamshells and associated gold collectors. As a consequence, we utilized low-cost aluminum collectors for the second LDEF tray (Figure 1b). Commercial series 1100, tempered grade aluminum (>99% pure) was used. The total tray surface was occupied by six individual panels (each approximately 41 x 46 cm and 3.2 mm thick) for a cumulative surface area of 1.1 m^2. It was clearly recognized from the beginning that compositional analyses might be limited on these aluminum targets compared to the gold substrate, but it was also thought that lower shock stresses induced by aluminum might lead to less vaporization, yielding relatively large quantities of melt that should not be intolerably contaminated by target impurities.

Instrument Locations

Recent theoretical work (refs. 10, 11) points out that effective particle fluxes and velocity distributions strongly depend on instrument orientation relative to the velocity vector of a non-spinning spacecraft, such as LDEF or Space Station. These new insights were not part of the initial LDEF or CME rationale, yet they are paramount in understanding the cratering record on LDEF and associated implications for the dynamics of the hypervelocity environment in LEO. A number of groups (Zook; McDonnell; Humes) have therefore engaged in similar, yet complementary and in part refined calculations, as did we during the concept development of future dust collection experiments on the Space Station Freedom.

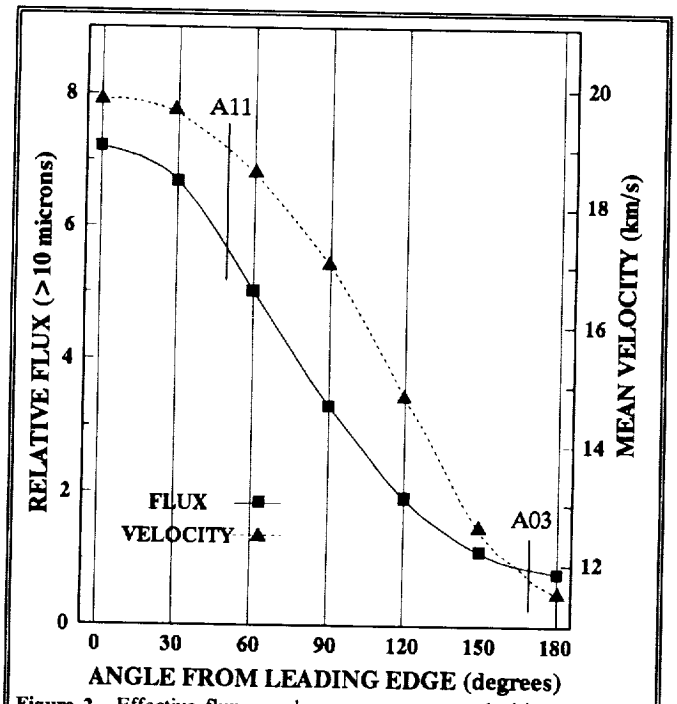

Figure 2. Effective fluxes and mean encounter velocities of natural and man-made particles >10 μm as a function of viewing direction on a non-spinning platform in LEO. The initial conditions underlying these calculations are largely those of reference 10.

Figure 2 illustrates some first order, general results and depicts the effective fluxes and mean velocities of natural particles >10 μm that encounter flat, vertical surfaces of specific, orientations relative to LDEF's velocity vector. Note that mean encounter velocities range from approximately 20 to 11 km/s for surfaces that point into the ram and anti-ram direction, respectively. Also note that the effective fluxes between those orientations may differ by a factor of 10. Because most impact damage is proportional to the impactor's kinetic energy, the combination of flux and mean velocities results in factors of 30 to 40 differences in the energy flux between ram and anti-ram directions, a substantial difference for the design and operation of flight systems. These model predictions may be tested by a wide variety of LDEF surfaces. Indeed, first order comparisons are being offered in this volume by most dust investigators.

CRATER POPULATIONS

All CME surfaces deemed useful to obtain detailed crater statistics by optical methods have been examined at resolutions that appear consistent with the quality of their surface finish, none of which is of high quality. We avoided any finishing by grinding and polishing for fear of contaminating the surfaces with embedded polishing compounds. The finishes on both surfaces were obtained by rolling processes, with the aluminum surfaces modestly improved and more homogenized after anodizing, using a sulfuric acid bath. The optical equipment and procedures used for crater counting are the same ones used during the KSC surveys by the M&D SIG (ref. 12). The actual diameters measured were rim-to-rim widths (D_r) for consistency (ref. 12), and because true crater diameters (D_c) (defined as the intercept of the crater wall with the flat target surface) are difficult to determine, especially for relatively small craters.

The crater counts are detailed in Figure 3 and summarized in Figure 4. The reasons for including all tray lips in these investigations are as follows: First, they represent substantial surface areas, each approximately 0.14 m^2, and deserve documentation in their own right. Second, they are manufactured from aluminum alloy 6061-T6, the only material common to both CME trays, and thus important for checks of internal self-consistency among our own surfaces and especially for comparison with other aluminum 6061-T6 surfaces that abound on LDEF (*e.g.*, ref. 13). This alloy is used widely on other spacecraft as well, the reason why its impact behavior is relatively well documented (*e.g.*, refs. 13, 14). The conversion of crater diameters to projectile dimensions and ultimately to mass should, therefore, be the most reliable for the Al-6061 tray lips. The actual collector materials composing CME are not as well calibrated as the tray lips, yet they should have experienced identical particle fluxes for the A03 and A11 locations. Analysis of the tray lips may thus provide internal consistency checks for the calibration and interpretation of crater diameters that accumulated on the CME collectors.

The crater statistics on the A03 tray lips also assume a pivotal role in explaining the "opened" clamshell configuration during retrieval by STS 32. These lips were continuously exposed throughout the total LDEF mission, but a nominally operating clamshell device permitted the gold collectors to be exposed only part of this time. As a consequence, the ratio of absolute crater densities on both surfaces is a direct measure of the fractional time during which the clamshells were in the open configuration.

Note in Figures 3 and 4 that the A11 tray crater densities are systematically higher than those of the A03 tray, for both the lips as well as the collector surfaces. This difference is ascribed to instrument orientation relative to LDEF's velocity vector as expected from Figure 2. The average flux in the forward-facing direction is distinctly higher than on the trailing edge.

The difference between the A03 tray lips and A03 collector data, however, cannot be due to instrument orientation. It must reflect difference in exposure time to an essentially identical impactor population. The modest crater concentrations of the gold collectors constitute first order evidence that the clamshells were not exposed continuously throughout the entire LDEF mission. The crater densities differ by approximately a factor of 2.

PROJECTILE POPULATIONS

Conversion of the crater diameter measurements to projectile diameters is a prerequisite to derive meaningful comparisons of particle fluxes and mass frequencies for LDEF instruments. Note that the average initial impact conditions will vary with specific LDEF location as suggested by Figure 2 and that we employed targets of different physical properties, the latter strongly controlling crater growth under otherwise identical conditions.

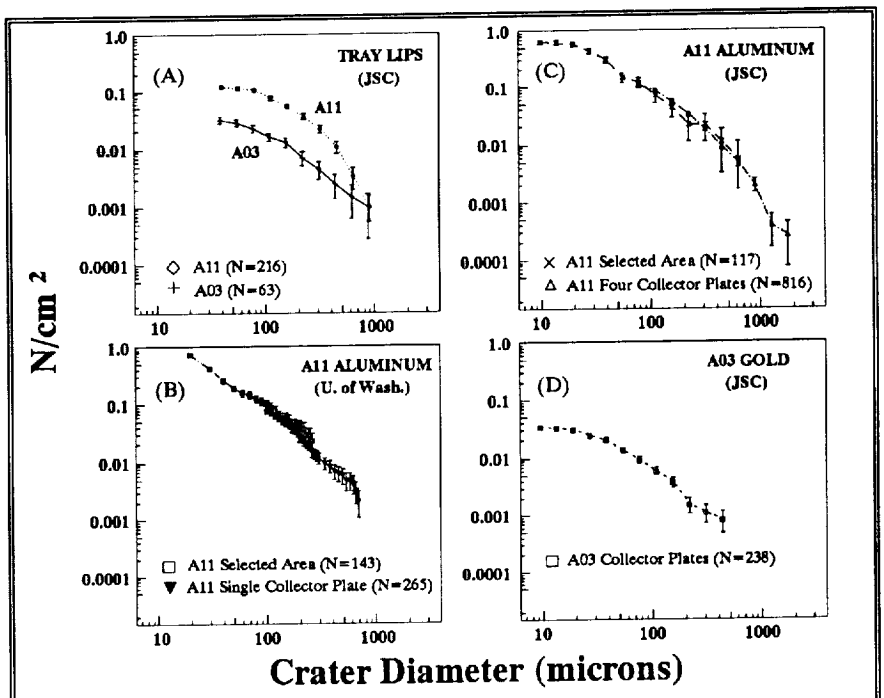

Figure 3. Detailed, optical crater counts performed on major CME surfaces. (A) Lips of instrument trays, composed of aluminum 6061-T6 measuring approximately 0.14 m^2 in surface area. These two surfaces best reflect the difference between rearward and forward-pointing directions, as the target materials were identical. (B) Crater counts on a single A11 aluminum plate (scanned at University of Washington). (C) Crater counts on a total of four A11 aluminum plates (scanned at JSC). (D) Crater counts on all gold surfaces (scanned at JSC). Error bars are statistical sampling errors (2 sigma).

We employed the experimentally determined crater scaling relationships derived by Cour-Palais (ref. 14) and as amended by E. Christiansen (personal communications, 1991) for all aluminum surfaces:

$$P=5.24D_p^{19/18}H^{-0.25}(d_p/d_t)^{0.5}(V/V_c)^{2/3} \qquad \text{(equation 1)}$$

where P is the crater depth, d_t and d_p the target and projectile densities (2.7 and 2.2 g/cm^3, respectively), H=Brinell hardness (90 and 40 for "6061-T6" and "1100, annealed" aluminum alloys, respectively); Vc=target sound velocity (6.1 km/s) and V=impact velocity (as extracted from Figure 2). Hemispherical crater profiles are typical for aluminum targets at light gas gun velocities, and crater diameter (D_c) thus relates to depth as $D_c=2P$, with both diameter and depth measured relative to the flat target surface (ref. 14). The actual measurement of rim diameter (D_r) converts to crater diameter D_c as

$$D_c=0.78\ D_r \qquad \text{(equation 2)}$$

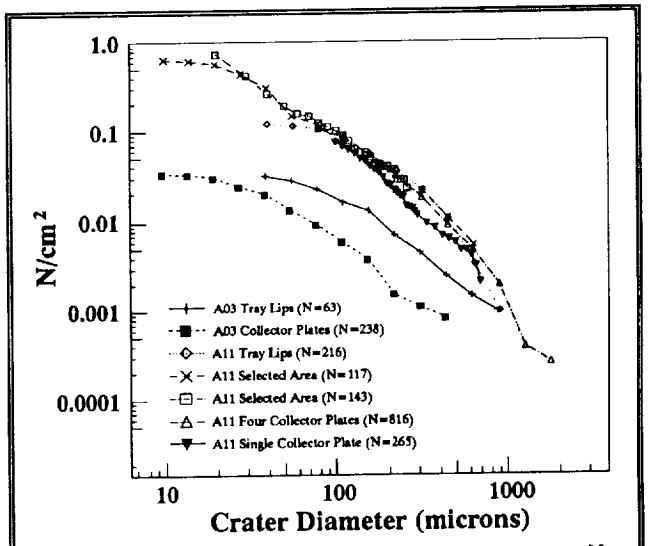

Figure 4. Summary comparisons of all CME crater counts. Note the general similarities in crater densities for all A11 surfaces that differ substantially from those of the A03 tray lips and gold surfaces. Differences among the A11 surfaces must be stochastic, yet the differences with and among the A03 surfaces relate to decreased effective flux and variable cumulative exposure time, respectively.

The latter derives from impact experiments, largely unpublished, into 1100 aluminum (ref. 15), which also found substantial agreement with the scaling relationships (ref. 14) as expressed by equation 1.

Calibration of the Au craters is based on dedicated experiments conducted with an electrostatic dust accelerator at MPI, Heidelberg, Germany, and a small caliber light gas gun at EMU, Freiburg, Germany (*e.g.*, ref. 16). Based on these data (Figure 5) a ratio of $D_C/D_P=5.7$ was extrapolated for the gold collectors at average encounter speeds of approximately 12 km/s.

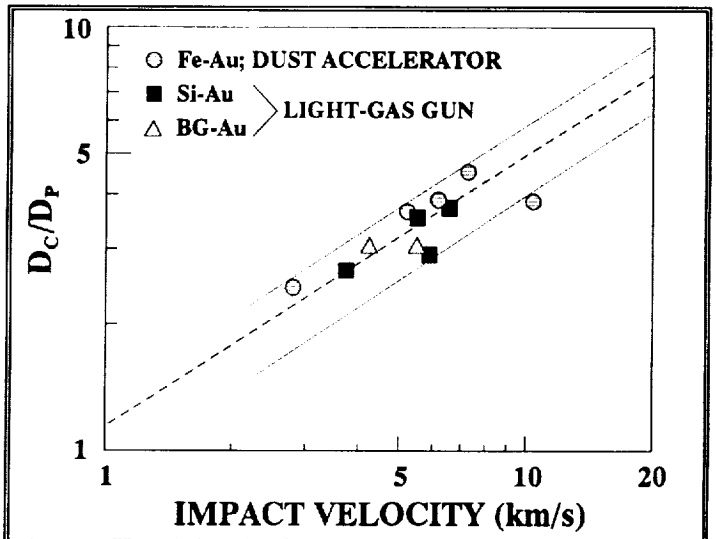

Figure 5. The relationship of crater diameter and impact velocity in gold targets based on micron-sized iron projectiles (electrostatic accelerator) and millimeter-sized glass projectiles (light gas gun).

Based on these crater scaling relationships, we converted the measured D_C or D_f into projectile diameters (D_P) and the results are presented in Figure 6. The following observations and possible interpretations are offered:

a) Note that similar absolute frequencies occur on all major A11 tray surfaces. The differences observed are within statistical error (Figure3) and we ascribe them to (expected) idiosyncrasies of the stochastic bombardment process.

b) The difference in effective flux between the A11 and A03 orientations, the major purpose of this plot, is somewhat difficult to quantify. We first note that the relative slopes of the A11 and A03 distributions seem to differ subtly, if taken at face value. However, if plotted in normalized form (not shown) and considering the statistical errors illustrated in Figure 3, the impactor size frequencies could be identical between the A11 and A03 orientations.

A statistically improved data set is needed to demonstrate whether the forward-facing surfaces do indeed experience larger numbers of "small" impactors compared to rearwards-pointing surfaces, the first order impression one derives from Figure 6. This impression, however, is not necessarily correct and could be driven by but a few random, "large" impacts on both surfaces. Note that the difference at the 100 μm projectile diameter is only a factor of 2-3 between the A11 and A03 orientations.

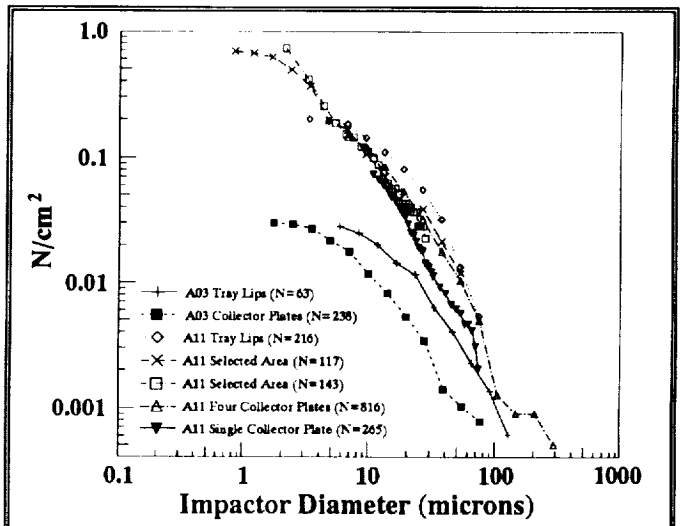

Figure 6. Projectile size frequency and relative flux for the statistically most valid CME surfaces.

Based on the above, we derived our best estimates for effective fluxes or relative exposure time from 20-30 μm diameter projectiles that correspond to craters of typically 100-180 μm in diameter, a size range that should be most representative and statistically valid, as it avoids the poor statistics at the large crater end and potential errors of omission at small crater sizes. Based on these qualifications, the A11 surfaces experienced approximately a factor of 8 larger flux than the trailing edge surfaces, a value modestly larger than that expected from Figure 2.

The effective cumulative exposure times between the A03 tray lip and gold collectors differ by approximately a factor of 2. A continuously cycling "active" instrument (see Appendix A) would expose the gold collectors for 1279 out of 2145 days, leading to a difference of 1.68 in cumulative exposure time. This ratio is modestly smaller than the factor of 2 difference in crater counts, yet within statistical error, the gold collector data indicate nominal instrument performance. If taken literally, the observed factor of 2 would imply even less exposure time than a nominally cycling instrument and would, therefore, result in a trend that is opposite the suspicion of a failed closing operation. We are

thus confident that the CME gold collectors were not exposed for any time longer than that allowed by an instrument that cycled repeatedly, by design, throughout the entire LDEF mission.

DEPTH/DIAMETER RATIOS OF CRATERS

Absolute crater depth is a complex function of target and projectile properties that control the target's penetration behavior and it depends strongly on absolute encounter velocity and impact angle (*e.g.,* refs. 14, 17, 18). Of course, these initial conditions also control the final crater diameter, leading to the concept of proportional crater cavity growth. This concept was adopted to convert measured crater diameters into associated projectile dimensions via equation 1. We measured the depth/diameter ratios of select craters primarily to test whether constant crater cavity geometries apply, and whether their average aspect ratios are consistent with the geometries assumed in equation 1.

We selected a single, random panel from the aluminum and gold collectors for this purpose and measured the depth of all craters >40 μm in diameter (*i.e.*, 174 impacts in aluminum and 26 in gold). The observed depth/diameter ratios vary considerably as illustrated in Figure 7.

The "standard" aspect ratio of $P/D_c=0.5$, derived from normal incidence laboratory experiments, does not apply even to averaged crater geometries. The aluminum craters are biased towards deeper structures than the standard crater, while the gold craters tend to be shallower. We tentatively interpret this difference with systematically different impact velocities (Figure 2). Also, small craters tend to display much larger ranges in P/D_c than larger structures, indicating substantially more variability for initial impact conditions among small projectiles. This could be due to increased variability in velocity, and especially in projectile density, the latter ranging from compact single minerals to relatively fluffy, low-density particles. Clearly, we do not understand these differences in detail, as a number of interdependent factors and parameters combine into the final crater shape. The data shown in Figure7 merely serve to illustrate the existence of large variability in P/D_c. Projectile properties based on a single diameter or depth measurement, and on an assumed and reasonable "average" initial impact conditions may yield highly model-dependent results. While Figure 7 seemingly points towards potential pitfalls of this approach, we are not in a position to suggest improvements.

CHEMICAL ANALYSIS OF PROJECTILE RESIDUES

We have performed a survey type assessment of the compositional make-up of particles by employing a Scanning Electron Microscope with an energy-dispersive X-ray analyzer. Most analyses to date are qualitative in the sense that they relate exclusively to the major elements present (>few percent) and that they address only their approximate proportions as deduced from visual inspection of associated X-ray spectra. This qualitative assessment suffices to survey the approximate composition of a large number of particles and to explore overall chemical variability. The deliberate tradeoff between analytical precision and total number of particles analyzed qualitatively is permitted at present to determine overall chemical variability, and to explore potential compositional groupings into distinct particle types. Quantitative analysis of every single particle is simply too time consuming and must be limited to representative specimen,

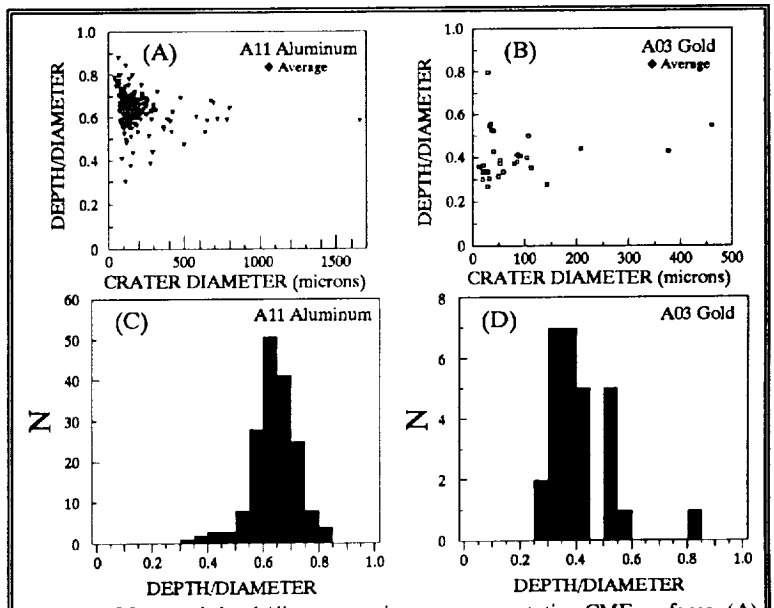

Figure 7. Measured depth/diameter ratios on representative CME surfaces. (A) and (B) display the measured ratios as a function of crater size for the A11 aluminum surfaces and the A03 gold collectors, respectively. Note the large scatter at small crater sizes. (C) and (D) are simple frequency histograms for the same surfaces. Note the bias towards relatively deep structures on the aluminum targets and towards unusually shallow structures on the gold collectors, none averaging $P/D_c=0.5$, the prevailing model assumption of a hemispherical crater cavity.

or those that are unusual by any number of criteria. Our CME approach was patterned after that developed during the analysis of Solar Max surfaces (refs. 19, 20), and after the preliminary investigation of stratospheric dust (ref. 21), all aimed at characterizing a large number of particles.

Figure 8 portrays crater morphologies and associated projectile residues. A few general comments apply. The presence of impactor residue is revealed with surprising ease during optical studies by a mostly dark coloration of the crater interiors. Craters which do not display dark crater bottoms or walls will generally not contain analyzable projectile residue. However, even dark crater liners are no guarantee that residues -- at the sensitivity levels of electron beam instruments -- are present; a fair fraction of craters that seemed promising optical candidates contained no analyzable residues.

A first order result of our compositional survey is that a significant fraction of the LDEF craters do not contain sufficient projectile remnants to be detected by the SEM methods that were employed (500 s and 30 KeV) in our initial survey. However, longer count times and higher accelerating voltages would provide better counting statistics, and thus, the resulting signal-to-noise ratio(s) might be sufficient to reveal minor traces of the impactor composition. This non-analyzable fraction of craters is >50%, even on the trailing edge gold surfaces, where mean velocities, shock stresses and temperatures are lowest. Compared to laboratory craters at 7 km/s (ref. 16), which yielded copious amounts of projectile melt, wholesale vaporization (or other loss mechanisms) seems to be common at the LDEF encounter speeds. Methods more sensitive than electron beam instruments, such as Secondary Ion Mass Spectrometry (SIMS and associated ion beams), are needed to possibly extract impactor compositions from many LDEF craters.

Projectile materials that we could detect and analyze with electron beam instruments occur commonly in the form of melts draping the crater walls or floors, mostly in the form of isolated patches, that seem to have contracted from very thin films by surface tension. Some melts have smooth surfaces, others are relatively rough and rich in vesicles. Also, genuine melt droplets occur frequently. The melt distribution inside crater cavities is generally very heterogeneous, rendering estimates about the mass fraction of the initial impactor that may be preserved in the crater interior highly impractical.

Some craters contain melts, as well as unmelted projectile fragments (Figure 8c). Such unmelted fragments are of special scientific value, as they may yield phase chemistries and mineralogic textural relationships that reflect their conditions of formation with substantially increased fidelity compared to the wholesale melts and associated average bulk compositions. The limited observations that we have on such unmelted fragments indicate mostly monomineralic compositions of olivine and pyroxene (Figure 9). It is known that olivine and pyroxene are more resistant to shock melting than many other rock-forming minerals (*e.g.,* ref. 22) and that fine-grained components melt more rapidly than coarse materials, especially if the fine-grained fraction is loosely packed and displays porosity (*e.g.,* refs. 23, 24,25). Most unmelted relicts have surprisingly uniform grain size (Figure 8c), possibly suggesting the breakup of one or more very large crystals. The presence of monomineralic relicts in a host melt of essentially chondritic average composition (Figure 9) is consistent with shock pressures in the 70-100 GPa range, mandating low impact velocities for the fragment-laden craters. Nevertheless, unmelted impactor fragments occur on both the trailing edge and forward-facing collectors, despite their substantially different mean encounter velocities. The presence of unmelted projectile materials following hypervelocity impacts into metallic targets is an important finding in view of future dust collections contemplated for Space Station that may employ somewhat improved collector media (*e.g.,* ref. 26).

We have analyzed approximately 300 LDEF craters and have found the compositional classifications and associated criteria developed during the analysis of the Solar Max surfaces (ref. 20) highly suitable for the classification of LDEF craters as well. We delineated three major groups of natural cosmic particles, in agreement with stratospheric particle populations (ref. 21).

The first group is dominated by Mg, Si and Fe, with Al, Ca and S as minor components. These are roughly "chondritic" compositions, typical for fine-grained, primitive meteorite matrices, as well as for many stratospheric particles (*e.g.,* refs. 1, 2, 27; Figures 8a, b and c). The next group is composed predominantly of Mg, Si, and Fe, with some variations in the Mg/Fe ratio. Such compositions are typical for monomineralic, mafic minerals, such as

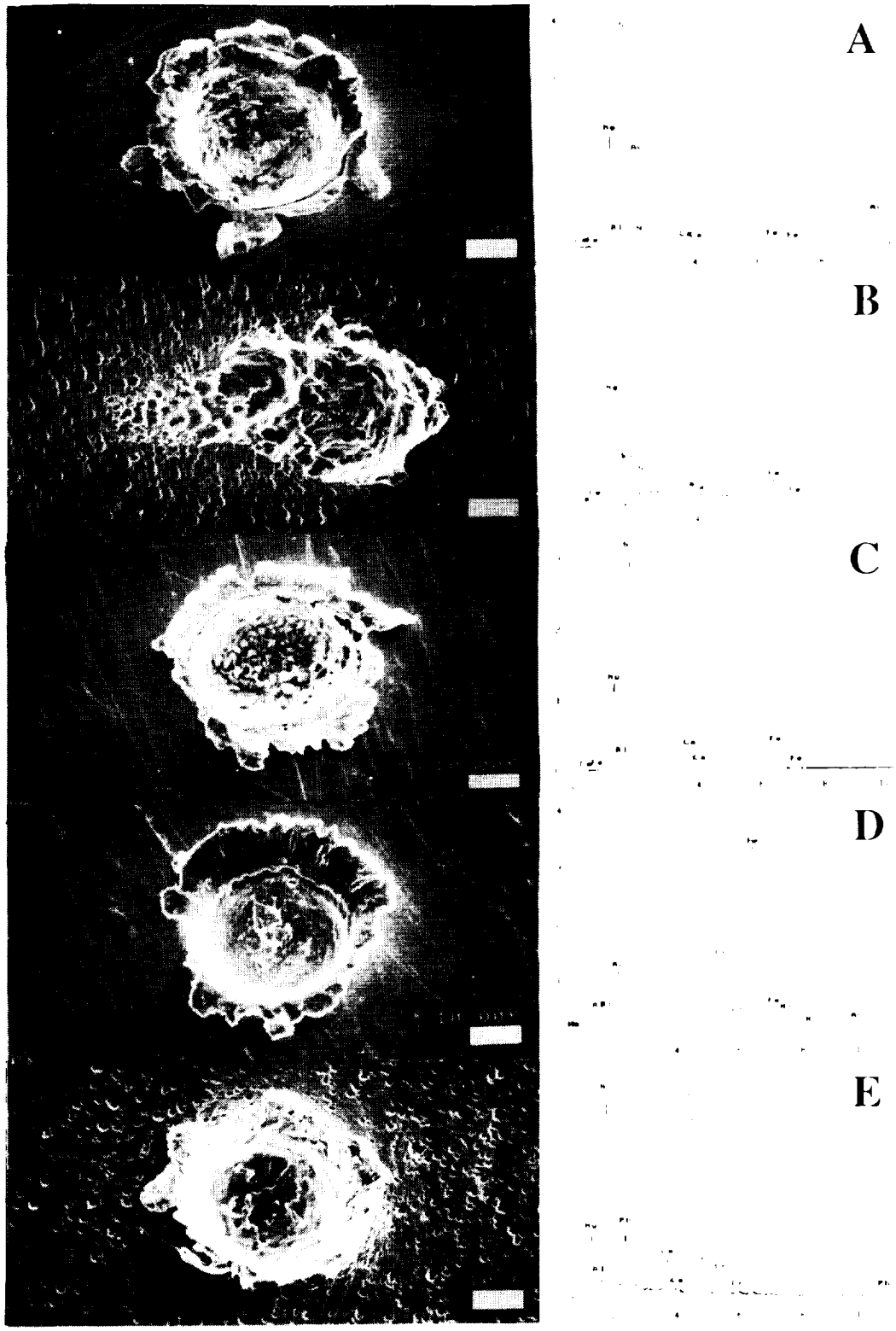

Figure 8. Representative morphologies of hypervelocity impact craters and associated X-ray spectra of projectile residues. (A) A "chondritic" impactor melt drapes the bottom and walls of a typical LDEF crater formed in gold, as evidenced by traces of the target substrate in the X-ray spectrum; (B) An unusually shallow and elongated crater indicative of a highly oblique impact angle by a natural impactor of chondritic composition; (C) Example of a rare crater displaying unmelted fragments of pyroxenes, all of relatively uniform grain size, residing in a host melt of chondritic composition (not illustrated); (D) Man-made debris (stainless steel) impact on trailing-edge gold substrate; (E) impact caused by paint flake on aluminum collector.

pyroxenes and olivines, known also from stratospheric dust or a variety of meteorites (*e.g.*, refs. 27, 28). As described above, most unmelted residue falls into this category, but most of the host melts are of chondritic composition and the entire particle would, therefore, be classified as chondritic. The third particle class is essentially monomineralic and represents Fe-Ni-rich sulfides, also known as discrete phases from carbonaceous chondrites and stratospheric particles (*e.g.*, ref. 27). Therefore, particle types 1-3 observed in LDEF craters resemble those recognized in the stratospheric dust collections or primitive meteorites. This assignment to otherwise unspecified "natural" sources rests heavily on current cosmic dust and meteorite research, as well as on general geochemical and petrological arguments applicable to natural silicate systems.

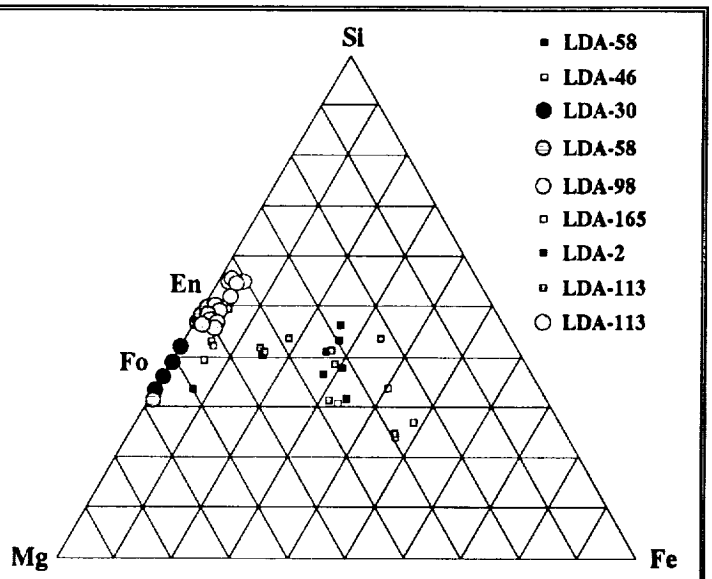

Figure 9. Quantitative analyses of select residues of natural projectiles that occurred in the form of unmelted fragments of pyroxene or olivine, typically associated with wholesale melts of different (chondritic) bulk composition that most likely reflect the particles' fine-grained matrices. Large circles reflect "monomineralic", unmelted fragments, while small squares represent the composition of melts. Note that some melts may have nearly monomineralic composition, a common occurrence in shocked, particulate targets.

Compositions that do not fall into any of the above three categories are strong candidates for man-made projectiles, as has been argued in the Solar Max case as well (refs. 19, 20). Most cannot be derived from silicate melts typical of geologic systems or from vapors that have elemental abundances similar to the overall solar system (*e.g.*, ref. 5). Any particle dominated by Fe, yet also containing substantial amounts of Ni and Cr (Figure 8d) does not seem to be a natural material on geochemical grounds, but must be interpreted as stainless steel on account of the high Cr content. Also, a particle almost exclusively made up of Ti and Pb (Figure 8e) seems incompatible with any reasonable natural substance, yet is a good match for paint pigments. Indeed, many particles of mono-elemental compositions seem excellent debris candidates, as are particles devoid of Si. In brief, substantial geochemical and petrogenetic arguments combined with knowledge of the sorts of man-made materials that exist in LEO can be used to distinguish between natural and man-made projectiles on a case by case basis. On occasion this distinction becomes difficult. For specific endmember compositions the distinction is easy, and in most cases assignment to natural and man-made sources can be made with confidence. We do not, at this time, present specific subgroups of man-made debris, because they display much more chemical variety than natural projectiles. Clearly, some groupings such as pure metals, alloys, and non-metals such as paints or composites, may be recognized with an increased data set.

Figure 10a relates to the rearward-facing gold collectors. It represents a complete survey of all craters >50 μm in diameter, combined with a representative set (approximately half of the total population) of craters between 20 and 50 μm, as well as some samples (~20% of observed population) between 10 and 20 μm. None of the <50 μm craters were selected on the basis of color or any other criterion, because we desired to analyze a "representative" suite of craters (in contrast to the Aluminum collector surfaces described below).

Note in Figure 10a the large fraction of craters that did not contain residue (134 of a total population of 196); even large structures may not possess analyzable residues. Approximately 1/3 (21 of 62) of the craters that do contain residue were caused by man-made debris; this represents approximately 10% of the total crater population on the gold collectors studied to date. This is an unexpectedly high number of man-made impactors on LDEF's trailing edge, where orbital debris contributions should be vanishingly small (*e.g.*, refs. 10, 11). It appears that contributions from highly elliptic orbits (geosynchronous sources) may have been underestimated in the past, a potentially significant result for orbital debris concerns. This conclusion, however, remains tentative until we and others confirm and quantify the possible flux of debris particles on LDEF's trailing edge. Indeed, the active Interplanetary Dust Experiment (IDE; ref. 29) advocates independently the existence of a co-orbiting dust cloud that impinged on their rearwards-pointing LDEF sensors. This cloud is interpreted as man-made debris on dynamic grounds by the original workers (ref. 29), yet others

have suggested a natural source (ref. 30). Regardless, our chemical analyses reveal debris impacts on LDEF's trailing edge supporting, at least in part, the largely dynamic arguments and conclusions derived from IDE.

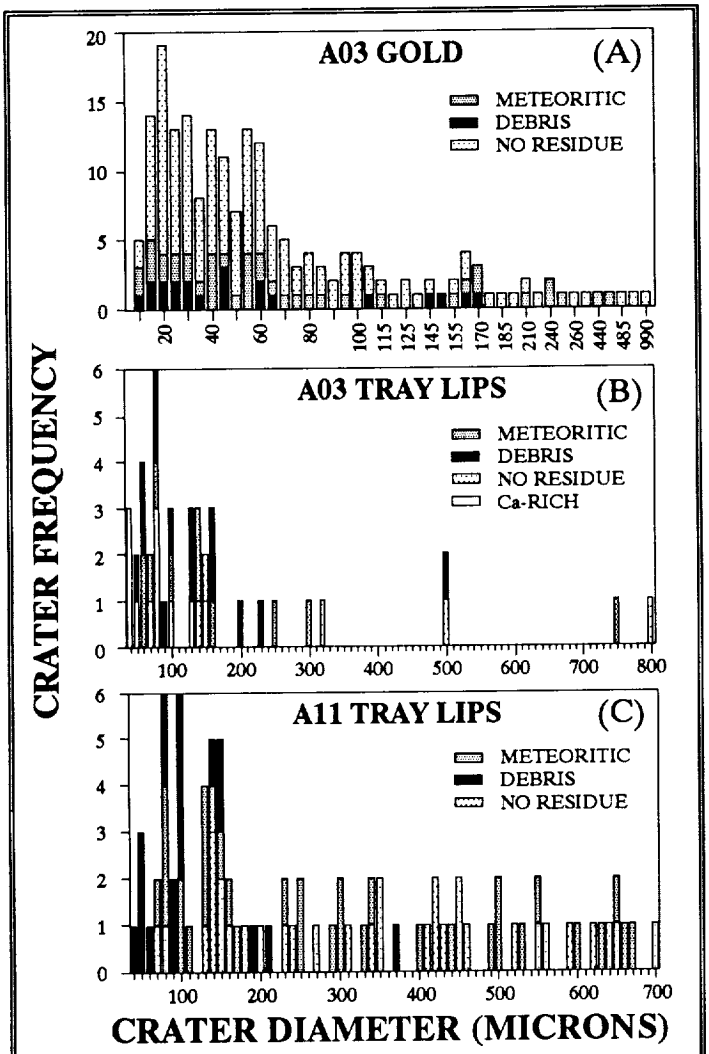

Figure 10. Overview of CME crater populations and associated projectile sources, arranged by crater size. (A) CME gold collectors; (B) A03 tray lips and (C) A11 tray lip. Note the presence of man-made debris on LDEF's trailing edge and the preponderance of debris particles producing "small" craters, especially on the A11 tray lip. For detailed classification criteria and other discussions see text.

We now turn to Figure 10b which depicts the current status of projectile analysis on the A03 tray lips, also pointing into the trailing direction. However, the statistics are not necessarily representative. These lips were our test surface used to sharpen analytical procedures, yet their intrinsic contaminants (total of 2.2%) provide omnipresent noise and background problems, and especially Fe and Ca are heterogeneously distributed throughout the alloy. In addition, these surfaces were contaminated with outgassed RTV or thermal paint forming Si and Ca-rich deposits (ref. 31), and abundant Na and Cl, including NaCl crystals derived during ground handling at KSC. We analyzed all craters >100 μm, but only optically promising candidates (dark colored liners) for structures <100 μm in diameter on the A03 tray lips.

Again, we observe man-made debris particles on a trailing edge surface, constituting approximately 1/3 of all craters >100 μm, but an ill-defined fraction of the craters <100 μm. Note that we distinguish a "Ca-rich" class of craters on the A03 tray lips. The Si-Ca-rich outgassing deposits (ref. 31) drape some craters to the degree that their signal totally overpowers any potential projectile residue. Quite frequently, this material is asymmetrically distributed in individual craters consistent with macroscopic evidence of highly laminar flow for the so called "nicotine" stains. The presence of this deposit in a fair number of craters must have implications to the temporal history of outgassing of diverse materials on LDEF.

The analyses of the A11 tray are illustrated in Figure 10c. In this case, we analyzed every crater >500 μm and a selected population of optically promising residue candidates at smaller sizes, which included basically all candidates >100 μm in diameter and a randomly selected fraction of candidates at <100 μm in diameter. Due to these selection procedures, the observations on A11 may not be readily compared with the A03 observations. Nevertheless, the ratio of natural to man-made particles seems modestly higher on the forward-facing tray, approximately 40% of all analyzable residues (yet an undefined fraction of the total). We have not analyzed, in systematic fashion ,the crater populations on the Al 1100 collector surfaces of the A11 tray.

In summarizing Figure 10 it appears that "large" craters seem to be predominantly the result of natural impactors. The largest debris craters have diameters of 220, 500 and 370 μm on the gold collectors, and the A03 and A11 tray lips, respectively (Figure 10). This size-dependent effect is particularity pronounced on the A11 tray lip, where "small" craters are distinctly biased towards man-made particles. This may be consistent with the observed projectile size frequencies (Figure 5) that may indicate increased numbers of "small" debris particles in the forward direction.

SUMMATION

This report summarizes the current status of the analysis of the Chemistry of Micrometeoroid Experiment. All optical characterizations are substantially complete, but chemical analysis of projectile residues has just begun.

The optical studies yield spatial densities of craters and resulting relative particle fluxes in substantial agreement with existing dynamic models in that effective fluxes are higher by a factor of approximately 8 in the A11 forward-facing direction. Also, the size or mass frequency of impactors seems to vary and the forward-pointing directions seem to experience numerous, additional small particles which we ascribe to man-made sources. Furthermore, the depth-diameter investigations seem to suggest substantially more variability in the initial impact conditions among "small" impactors, such as widely differing encounter velocities and a wide range in projectile densities, compared to more massive projectiles (*e.g.*, ref. 13). These findings, on an individual experiment, exposed in two different orientations relative to LDEF's velocity vector, demonstrate the significant advances that can be made from the analysis of all LDEF surfaces to improve our understanding of most aspects of the hypervelocity particle environment in LEO.

The chemical analyses concentrated on survey-type assessment of compositional variability among all impactors. Three major types of natural cosmic-dust particles could be identified: 1) particles of "chondritic" compositions; 2) monomineralic, mafic silicates such as olivines and pyroxenes; and 3) Fe-Ni sulfides. These particle types have strong affinities to those observed in the stratospheric dust collections. We also observed man-made debris particles, such as metals and paint flakes. However, at present we are unable to specify the relative abundance of man-made and natural particles in LEO. On the one hand, our analyses are not sufficiently systematic, and on the other hand, we cannot characterize the impactors for >50% of all craters, because their residues, if present, are below the detection limit for the electron beam instrument(s) and methods employed. More sensitive analytical methods, such as SIMS, are needed to obtain a more complete overview of impactor compositions and potential origins.

Nevertheless, two important results emerged from these preliminary SEM analyses. We found unmelted fragments of olivine and pyroxene, a discovery that substantiates the expectation that unmelted impactor fragments may be recovered by improved capture media on future dust experiments in LEO. The other significant result relates to the presence of man-made debris on the trailing edge, which suggests that the role of particles in highly elliptical orbits from geosynchronous sources may have been underestimated in the past.

ACKNOWLEDGEMENTS

Many individuals contributed to the design and manufacture of CME, including J. Joerns, R. Chandler, R. Scimek, and D. Demonburn, most of them retired, attesting to LDEF's longevity and endurance. Retrieval, deintegration and collector processing benefitted greatly from their advice and the skills by W. Brown, F. Cardenas, W. Davidson and G. Haynes, all of Lockheed, Houston. Lastly, without the guidance, persistence, and collaborative spirit of a dedicated LDEF staff at LaRC, foremost W. Kinard and J. Jones, this experiment and LDEF would not have been successful. Over the life span of LDEF, our scientific thinking evolved measurably thanks to numerous exchanges with M. Cintala, D. McKay, M. Zolensky, H. Zook, and many other individuals. We are grateful to all of them.

REFERENCES

1) Brownlee, D.E., Tomandl, D.A., and Olsewski, E. (1977), Interplanetary dust: a new source of extraterrestrial material for laboratory study. *Proc. Lunar Sci. Conf., 8th*, p. 149-160.

2) Brownlee, D. E. (1985) Cosmic Dust: Collection and Research, *Ann. Rev. Earth Planet. Sci. 13*, p. 134-150.

3) Bradley, J.P., Sanford, S.A., and Walker, R.M. (1988) Interplanetary Dust Particles, In *Meteorites and the Early Solar System*, J. Kerridge and M. Matthews, eds., Univ. Arizona Press, p. 861-898.

4) Zinner, E. (1988) Interstellar Cloud Material in Meteorites, in *Meteorites and the Early Solar System*, J. Kerridge and M. Matthews, eds., Univ. Arizona Press, p. 956-984.

5) Kerridge, J. and M. Matthews, eds. (1988) *Meteorites in the Early Solar System*, Univ. of Arizona Press, 1988, 1269 pp.

6) Kissel, J. and 18 coauthors (1986) Composition of comet Halley dust particles from Giotto observations, *Nature, 321*, p. 336-337.

7) Kessler, D.J. (1991) Orbital Debris Environment for Space Craft in Low Earth Orbit, *J. Spacecraft, 28, 3*, p. 347-351.

8) Tsou, P.(1990) Intact capture of hypervelocity particles, *Int. J. Impact Engng., 10*, p. 615-627.

9) Barrett, R.A., Zolensky, M.E., Lindstrom, D.J., Gibson, E.K. and Hörz, F. (1991) Suitability of Silica Aerogel as a capture medium for interplanetary dust, *Proc. Lunar Planet. Sci. Conf. 22nd*.

10) Zook, H.A. (1991) Meteoroid Directionality on LDEF and Asteroidal versus Cometary Sources (abstract), *Lunar Planet. Sci. XXII*, p. 1577-1578.

11) Kessler, D.J, Reynolds, RC. and Anz-Meador, P.D. (1988) *Orbital Debris Environment for Spacecraft Designed to operate in Low Earth Orbit, NASA TM-100-471*, April 1988.

12) See, T.H., Allbrooks, M., Atkinson, D., Simon, C. and Zolensky, M. (1990) *Meteoroid Impact and Debris Impact Features Documented on the Long Duration Exposure Facility*, Johnson Space Center (JSC) Publication # 24608, 583 pp.

13) Humes, D.H. (1991) Large craters on the Meteoroid and Space Debris Impact Experiment, *1st LDEF Symposium, NASA CP-*3134, 1992.

14) Cour-Palais, B.G. (1987) Hypervelocity Impacts in Metals, Glass, and Composites, *Int. J. Impact Engng., 5*, p. 681-692.

15) Hörz, F., Messenger, S., Bernhard, R., See, T.H. and Haynes, G. (1991) Penetration phenomena in Teflon and aluminum films using 50-3200 μm glass projectiles, *Lunar Planet. Sci. Conf. 22nd*, Abstracts, Lunar and Planetary Institute, p. 591-592.

16) Hörz, F., Fechtig, H. and Janicke, J.(1983) Morphology and chemistry of projectile residue in small experimental impact craters, *Proc. Lunar Planet. Sci. Conf. 14th, J. Geophys. Res., 88*, p. B353-B363.

17) Gault, D.E. (1973) Displaced mass, depth, diameter, and effects of oblique trajectories for impact craters formed in dense crystalline rock, *The Moon, 6*, p. 32-44.

18) Pailer, N. and Grün, E. (1980) The penetration limit of thin films, *Planet. Space. Sci., 28*, p. 321-331.

19) Warren, J.L. and 10 co-authors, (1989) The detection and observation of meteoroid and space debris impact features on the Solar Max satellite, *Proc. Lunar Planet. Sci. Conf., 19th*, p. 641-657.

20) Rietmeijer, F.J.M., Schramm, L., Barrett, R.A., McKay, D.S. and Zook, H.A. (1986) An inadvertent capture cell for orbital debris and micrometeoroids; the Main Electronics Box thermal blanket of the Solar Maximum Satellite, *Adv. Space. Res., 6*, p. 145-149.

21) Zolensky, M.E. ed. (1990), *Cosmic Dust Catalog, 11, 1*, Particles from Collection Flag L2005, JSC # 24461-SN-83, 170 pp.

22) Stöffler, D. (1972) Deformation and transformation of rock-forming minerals by natural and experimental shock processes; behavior of minerals under shock compression, *Fortschr. Mineral., 49*, p. 50-113.

23) Kieffer, S.W. (1971) Shock metamorphism of the Coconino Sandstone at Meteor Crater, Arizona, *J. Geophys. Res. 76*, p. 5449-5473.

24) Schaal, R.B., Hörz, F., Thompson, T.D. and Bauer, J.F. (1979) Shock metamorphism of granulated lunar basalt, *Proc. Lunar Planet. Sci. Conf., 10th*, p. 2547-2571.

25) Simon, S.B., Papike, J.J., Hörz, F. and See, T.H. (1985) An experimental investigation of agglutinate melting mechanisms: shocked mixtures of sodium and potassium feldspars, *Proc. Lunar Planet. Sci. Conf., 16th, J. Geophys. Res., 90*, p. D103-D115.

26) Hörz, F. ed. (1990) *Cosmic Dust Collection Facility: Scientific Objectives and Programmatic Relations, NASA TM 102160*, 1990, pp.29.

27) MacKinnon, I.D.R. and Rietmeijer, F.J.M. (1987) Mineralogy of chondritic interplanetary dust particles, *Rev. Geophys. Space Phys., 25*, p. 1527-1553.

28) Klock, W., Thomas, K.L., McKay, D.S. and Palme, H. (1989) Unusual olivine and pyroxene composition in interplanetary dust and unequilibrated ordinary chondrites, *Nature, 339, No 6220*, p. 126-128.

29) Mullholland, J.D. and 8 co-authors (1991) IDE Spatio-temporal fluxes and high time-resolution studies of multi-impact events and long-lived debris clouds, *1st LDEF Symposium, NASA CP-*3134, 1992.

30) McDonnell, J.A.M. and Sullivan, K. (1991) Dynamic (computer) modelling of the particulate environment: Transformations from the LDEF reference frame to decode geocentric and interplanetary populations, *1st LDEF Symposium, NASA CP-*3134, 1992.

31) Crutcher, E.R., Nishimura, L.S., Warner, K. and Wascher, W.W. (1991) Migration and generation of contaminants from launch through recovery: LDEF Case History, *1st LDEF Symposium, NASA CP-*3134, 1992.

APPENDIX A

The Problem

The active experiment (A03) employed two pairs of moveable clamshell-type devices that were closed at the time of LDEF deployment, but were scheduled to open approximately 10 days later. Nominal closing was scheduled to occur on mission-day 298. However, the instrument was found to be open at the time of LDEF retrieval, giving rise to the possibility that the closing operation(s) failed.

Instrument Design

The two clamshell pairs were totally independent mechanically, each pair having its own driveshaft, motor, battery-power, etc. This redundancy permitted potential mechanical failure of one pair of clamshells, while the other pair could still function nominally. However, both motors were controlled from a single electronic sequencer, with the latter being powered from a third battery. The sequencer contained a hexadecimal clock of 256 time intervals, each interval lasting two days. During design of this system, no provision was made to prevent this clock from recycling after 256 intervals, (*i.e.*, 512 days) of mission elapsed time, because the retrieval of LDEF was scheduled much earlier. Therefore, by design, the instrument could open and close indefinitely, the only constraint being battery-lifetime to power the sequencer or motors.

Post-Flight Inspection

Both sets of clamshells were fully extended (i.e., open) and it appears unlikely that any mechanical failure occurred; there was no evidence that either pair attempted to close. In addition, all three batteries were found to be sufficiently

charged to service and drive all CME systems. Unfortunately, the original ground-support system(s) were not available at KSC in 1990, particular an external frequency generator used to speed up the internal clock during assembly and pre-launch tests. Furthermore, the designer of the sequencer was unavailable for consultation so there remains doubt as to whether suitable equipment, procedures, or both were used during these post-retrieval tests; the clock simply would not respond to the external signals. A modified procedure was devised that electrically bypassed the clock and that resulted in successful closure of the clamshells. The rate of clamshell movement was nominal, as were motor torques and start up amperages, attesting to the mechanical integrity of all systems, as well as the electrical systems, except for the clock. Following clamshell closure it became evident that interior surfaces of the instrument had been exposed to the space environment (*i.e.*, craters were observed). The latter demonstrates that the instrument must have been closed for some time, and precludes the possiblity that the clamshells remained open throughout the entire LDEF mission.

Diagnosis

There was no positive design feature to shut-off the internal clock after completion of the first closing-sequence (day 298), or after completion of the clock's first full cycle (day 512). All systems were permitted to operate indefinitely in cyclic fashion with battery-power being the only limiting factor. The deployed or open clamshells found during STS 32 retrieval operations are consistent with CME's cycle period; the battery status permitted multiple cycling as well. Craters found in the instrument interior demonstrate that opening, closing, and opening operations occurred at least once. The crater populations on the gold collectors relative to those on the continuously exposed tray lips are consistent with a continuously cycling CME, but are inconsistent with failure of a closing sequence. The evidence suggest that the active CME instrument was still functioning nominally at the time of LDEF retrieval.